

Comparison of triple quantum (TQ) TPPI and inversion recovery TQ TPPI pulse sequences at 9.4 and 21.1 T

Simon Reichert^{1,2,3}  | Victor Schepkin⁴ | Dennis Kleimaier¹  |
Frank G. Zöllner^{1,2,3} | Lothar R. Schad^{1,2}

¹Computer Assisted Clinical Medicine, Medical Faculty Mannheim, Heidelberg University, Heidelberg, Germany

²Mannheim Institute for Intelligent Systems in Medicine, Medical Faculty Mannheim, Heidelberg University, Mannheim, Germany

³Cooperative Core Facility Animal Scanner ZI, Medical Faculty Mannheim, Heidelberg University, Mannheim, Germany

⁴National High Magnetic Field Laboratory, Florida State University, Tallahassee, Florida, USA

Correspondence

Simon Reichert, Cooperative Core Facility Animal Scanner ZI, Medical Faculty Mannheim, Heidelberg University, Mannheim, Germany.
Email: simon.reichert@medma.uni-heidelberg.de

Funding information

German Research Foundation, Grant/Award Number: 410981386; National Science Foundation, Grant/Award Number: DMR-1644779; National High Magnetic Field Laboratory

Purpose: Both sodium T_1 triple quantum (TQ) signal and T_1 relaxation pathways have a unique sensitivity to the sodium molecular environment. In this study an inversion recovery time proportional phase increment (IRTQTPPI) pulse sequence was investigated for simultaneous and reliable quantification of sodium TQ signal and bi-exponential T_1 relaxation times.

Methods: The IRTQTPPI sequence combines inversion recovery TQ filtering and time proportional phase increment. The reliable and reproducible results were achieved by the pulse sequence optimized in three ways: (1) optimization of the nonlinear fit for the determination of both T_1 -TQ signal and T_1 relaxation times; (2) suppression of unwanted signals by assessment of four different phase cycles; (3) nonlinear sampling during evolution time for optimal scan time without any compromises in fit accuracy. The relaxation times T_1 and T_2 and the TQ signals from IRTQTPPI and TQTPPI were compared between 9.4 and 21.1 T. The motional environment of the sodium nuclei was evaluated by calculation of correlation times and nuclear quadrupole interaction strengths.

Results: Reliable measurements of the T_1 -TQ signals and T_1 bi-exponential relaxation times were demonstrated. The fit parameters for all four phase cycles were in good agreement with one another, with a negligible influence of unwanted signals. The agar samples yielded normalized T_1 -TQ signals from 3% to 16% relative to single quantum (SQ) signals at magnetic fields of both 9.4 and 21.1 T. In comparison, the normalized T_2 -TQ signal was in the range 15%–35%. The TQ/SQ signal ratio was decreased at 21.1 T as compared with 9.4 T for both T_1 and T_2 relaxation pathways. The bi-exponential T_1 relaxation time separation ranged from 15 to 18 ms at 9.4 T and 15 to 21 ms at 21.1 T. The T_2 relaxation time separation was larger, ranging from 28 to 35 ms at 9.4 T and 37 to 40 ms at 21.1 T.

Conclusion: The IRTQTPPI sequence, while providing a less intensive TQ signal than TQTPPI, allows a simultaneous and reliable quantification of both the T_1 -TQ signal and T_1 relaxation times. The unique sensitivities of the T_1 and T_2 relaxation pathways

Abbreviations: DQ, double quantum; EFG, electric field gradient; FID, free induction decay; FT, Fourier transform; (IRTQTPPI, (inversion recovery) time proportional phase increment; ISTO, irreducible spherical tensor operator; SAR, specific absorption rate; SNR, signal to noise ratio; SQ, single quantum; TQ, triple quantum; TQF, TQ filtering; T_R , repetition time; TSC, tissue sodium concentration; ZQ, zero quantum.

This is an open access article under the terms of the [Creative Commons Attribution-NonCommercial-NoDerivs](https://creativecommons.org/licenses/by-nc-nd/4.0/) License, which permits use and distribution in any medium, provided the original work is properly cited, the use is non-commercial and no modifications or adaptations are made.

© 2024 The Authors. *NMR in Biomedicine* published by John Wiley & Sons Ltd.

to different types of molecular motion provide a deeper understanding of the sodium MR environment.

KEYWORDS

^{23}Na (sodium) MRI, inversion recovery, multi-quantum, T_1 and T_2 relaxation, triple quantum (TQ)

1 | INTRODUCTION

The ^{23}Na nucleus provides not only the second strongest biological MR signal but also has attractive biomedical and physical properties.^{1,2}

Sodium ions are involved in multiple vital cell processes, such as membrane transport processes and electric signaling between neurons.³ The sodium–potassium pump maintains a large concentration gradient between intra- and extracellular space by constantly pumping sodium ions out of the cell and potassium ions into the cell.^{4,5} The energy consumption of this process is up to two-thirds of the cell's total energy. This combined with the crucial involvement of the sodium concentration gradient in cellular transport processes and electric signaling between cells demonstrates the vital importance of the sodium–potassium pump for cell viability. Insufficient energy supply leads to a failure of the sodium–potassium pump followed by an influx of water and sodium ions into the cell. Thus, changes in the intracellular sodium concentration correlate with early pathophysiological changes.

The single quantum (SQ) ^{23}Na MR signal, that is, the tissue sodium concentration (TSC), represents the mean of the intra- and extracellular sodium concentrations.^{1–3,6,7} The TSC provides valuable information about cell viability and physiology. However, the SQ signal does not allow us to differentiate between increased intracellular sodium concentration and increased extracellular volume (for example, during cell shrinking).⁸ The triple quantum (TQ) signal, on the other hand, has been proven to provide a higher weighting toward intracellular sodium content compared with the SQ signal.^{9–16} This TQ signal is created during bi-exponential relaxation that results from slow interactions, that is, correlation times in the range of several nanoseconds to milliseconds of the sodium electrical quadrupole moment with surrounding electric field gradients (EFGs).^{3,17–21} Such interactions occur during sodium ion binding with proteins and other macromolecules.^{3,22} Several studies with perfused rat heart systems,^{9,13,14,23–25} brain ischemia²⁶ and tumors^{27,28} and in vitro experiments using MR-compatible bioreactor systems^{29–32} have demonstrated a correlation of the TQ signal with cell viability. The TQ signal increases with the intracellular sodium concentration¹⁴ and depends on the sodium^{9,14} and protein^{9,13} concentrations as well as the protein folding state.³³ Consequently, the TQ signal has been shown to be a valuable biomarker for cell viability.

Previous studies of the sodium TQ signal have mainly investigated the T_2 relaxation pathway, based on the evolution of the nuclear magnetization between states $T_{11} \leftrightarrow T_{31}$.^{14,15,22,30,31,33–40} An alternative pathway for the creation of the TQ signal uses T_1 relaxation based on the evolution $T_{10} \rightarrow T_{30}$.^{3,20} The T_1 -TQ signal is sensitive to an intermediate motional regime ($\omega_0\tau_c \sim 1$) compared with the slow motional regime ($\omega_0\tau_c \gtrsim 1$) of the T_2 -TQ signal.⁴¹ Thus, interaction durations in the range of a few nanoseconds dominate the T_1 -TQ signal. In contrast, the longer interaction times dominate the T_2 -TQ signal. Thus, the T_1 -TQ signal has a different sensitivity to environment and can provide valuable information to better characterize sodium–protein interactions. Such interactions are characterized by a wide range of correlation times. Hence, the investigation of both T_1 - and T_2 -TQ signals can advance our understanding of TQ signal formation in biological environments. However, only a few studies have been able to detect bi-exponential T_1 relaxation and/or a T_1 -TQ signal,^{42–44} as the fast T_{1f} relaxation time component contributes only 20% to the overall signal. Hence, evaluation of bi-exponential T_1 relaxation times and especially T_{1f} is difficult. Therefore, a reliable tool for investigation of the T_1 -TQ signal and the bi-exponential T_1 relaxation times is necessary to obtain a deeper understanding of ^{23}Na in biological tissue.

It is known that a direct MR detection of the TQ signal is not possible,¹⁷ and hence phase-cycling sequences, that is, TQ filtering (TQF) sequences, are often used.^{22,34,35,39,41} The basic T_2 -TQF sequence consists of three pulses with evolution periods between the pulses and an optional 180° RF pulse between the first and second pulses. The first RF pulse excites the spins followed by evolution to an intermediate T_2 -TQ state (T_{31}). The second RF pulse creates T_{33} coherences. This transformation also leads to a threefold increased accumulation of phase for the final output SQ signal. The interval between the second and third RF pulses, often called the mixing period, is usually set as short as possible to minimize T_2 -TQ signal decay. The last 90° RF pulse transforms the T_{33} coherence back into T_{31} coherence, which evolves to the detectable T_{11} coherence. To separate the T_2 -TQ signal from other MR signals, the phases of the RF pulses are changed in the subsequent repetitions of the RF pulse sequence.⁴¹

The detection of the T_1 -TQ signal requires a modified pulse sequence and phase cycling. Jaccard et al.⁴¹ have already proposed an inversion recovery TQ filtration (IR-TQF) pulse sequence using the T_1 relaxation pathway. In the case of imperfect inversion, the $T_{1\pm 1} \rightarrow T_{3\pm 1}$ and the $T_{10} \rightarrow T_{30}$ pathways indistinguishably contribute to the TQ signal.³ Moreover, unwanted signal contributions, for example, double quantum (DQ) signals, may overlap with the TQF signal, making TQ signal quantification a difficult task. Therefore, methods that suppress unwanted signal contributions may improve the quantification of the T_1 relaxation times and the T_1 -TQ signal.

Based on the sequence of Jaccard et al.,⁴¹ we propose an inversion recovery time proportional phase increment sequence (IRTQTPPI), which allows a simultaneous quantification of bi-exponential T_1 relaxation times and T_1 -TQ signal, similar to the TQTPPI sequence. To reliably detect the T_1 relaxation times and the T_1 -TQ signal, three different DQ suppression methods were evaluated using a simulation framework and experiments. The optimized IRTQTPPI sequence, T_{1-} and T_{2-} TQ signals were compared between 9.4 and 21.1 T for the agar tissue model system. The local motional environment was characterized by evaluating the correlation time and nuclear quadrupole interaction strength.

2 | THEORY

Sodium nuclei interact via electric quadrupole interaction with surrounding EFGs created by the molecular environment of the sodium ions. The ^{23}Na NMR dynamics are described by the Liouville equation $\frac{d\sigma}{dt} = -i[H, \sigma]$, where H is the Hamiltonian of the system under study. The density operator σ can be expressed in terms of irreducible spherical tensor operators T_{mn} (ISTOs),⁴⁵ that is, longitudinal magnetization is proportional to T_{10} and transversal magnetization to $T_{1\pm 1}$. Using the ISTO basis, the equation of motion becomes^{20,46}

$$\frac{d\sigma}{dt} = -i\bar{\omega}_Q [T_{20}, \sigma] - \sum_{n=-2}^2 [T_{2n}, [T_{2n}^\dagger, \sigma - \sigma_{\text{eq}}]] (J_n(\omega_0) + iK_n(\omega_0)), \quad (1)$$

where $\sigma_{\text{eq}} \sim T_{10}$ is the thermal equilibrium density operator and J_n are the spectral densities that encode the sodium molecular environment. The K_n value is negligible in most situations and only leads to an overall dynamic shift.

Under the common assumption^{3,20,22,33} of a single correlation time τ_c and a nucleus quadrupole interaction of strength ω_Q , the spectral densities J_n can be written as

$$J_n = \omega_Q^2 \frac{\tau_c}{1 + (n\omega_0\tau_c)^2}. \quad (2)$$

$\bar{\omega}_Q$ is the residual quadrupole coupling constant. This equation leads to a set of decoupled differential equations for each coherence order,^{20,46}

$$\frac{d}{dt} \begin{pmatrix} T_{10} \\ T_{20} \\ T_{30} \end{pmatrix} = \begin{pmatrix} \frac{2}{5}J_1 + \frac{8}{5}J_2 & 0 & \frac{4}{5}(J_1 - J_2) \\ 0 & 2(J_1 + J_2) & 0 \\ \frac{4}{5}(J_1 - J_2) & 0 & \frac{8}{5}J_1 + \frac{2}{5}J_2 \end{pmatrix} \cdot \begin{pmatrix} T_{10} \\ T_{20} \\ T_{30} \end{pmatrix} - \begin{pmatrix} \frac{2}{5}J_1 + \frac{8}{5}J_2 \\ 0 \\ \frac{4}{5}(J_1 - J_2) \end{pmatrix} \quad (3)$$

$$\frac{d}{dt} \begin{pmatrix} T_{1\pm 1} \\ T_{2\pm 1} \\ T_{3\pm 1} \end{pmatrix} = \begin{pmatrix} \frac{3}{5}J_0 + J_1 + \frac{2}{5}J_2 & \mp i\sqrt{3/5}\bar{\omega}_Q & \frac{\sqrt{6}}{5}(J_0 - J_1) \\ \mp i\sqrt{3/5}\bar{\omega}_Q & J_0 + J_1 + 2J_2 & \mp i\sqrt{3/5}\bar{\omega}_Q \\ \frac{\sqrt{6}}{5}(J_0 - J_1) & \mp i\sqrt{3/5}\bar{\omega}_Q & \frac{2}{5}J_0 + J_1 + \frac{3}{5}J_2 \end{pmatrix} \cdot \begin{pmatrix} T_{1\pm 1} \\ T_{2\pm 1} \\ T_{3\pm 1} \end{pmatrix} \quad (4)$$

In the case of isotropic environment, where $\bar{\omega}_Q = 0$, the Rank 2 coherences are decoupled from Rank 1 and 3 coherences. The analytical solutions for the above zero quantum (ZQ) and the SQ differential equations are

$$\begin{pmatrix} T_{10} \\ T_{30} \end{pmatrix} \rightarrow \begin{pmatrix} 1 - f_{11}^{(0)}(t) \\ -f_{13}^{(0)}(t) \end{pmatrix} + \begin{pmatrix} f_{11}^{(0)}(t) & f_{13}^{(0)}(t) \\ f_{31}^{(0)}(t) & f_{33}^{(0)}(t) \end{pmatrix} \cdot \begin{pmatrix} T_{10} \\ T_{30} \end{pmatrix} \quad (5)$$

$$\begin{pmatrix} T_{11} \\ T_{31} \end{pmatrix} \rightarrow \begin{pmatrix} f_{11}^{(1)}(t) & f_{13}^{(1)}(t) \\ f_{31}^{(1)}(t) & f_{33}^{(1)}(t) \end{pmatrix} \cdot \begin{pmatrix} T_{11} \\ T_{31} \end{pmatrix}. \quad (6)$$

For simplicity, the \pm signs in $T_{1\pm 1}$ and $T_{3\pm 1}$ are dropped. The bi-exponential ZQ transfer functions $f_{ij}^{(0)}(t)$ (Reference 20)

$$\begin{aligned}
 f_{11}^{(0)}(t) &= A_{1s} \exp\left(-\frac{t}{T_{1s}}\right) + A_{1f} \exp\left(-\frac{t}{T_{1f}}\right), \\
 f_{13}^{(0)}(t) = f_{31}^{(1)}(t) &= \frac{2}{5} \left(\exp\left(-\frac{t}{T_{1f}}\right) - \exp\left(-\frac{t}{T_{1s}}\right) \right) \\
 f_{33}^{(0)}(t) &= A_{1f} \exp\left(-\frac{t}{T_{1s}}\right) + A_{1s} \exp\left(-\frac{t}{T_{1f}}\right)
 \end{aligned} \tag{7}$$

correspond to longitudinal relaxation with relaxation times $T_{1s} = \frac{1}{2J_1}$ (slow) and $T_{1f} = \frac{1}{2J_2}$ (fast). The theoretical amplitudes $A_{1s} = 0.8$ and $A_{1f} = 0.2$ are the slow and fast components, respectively. The SQ transfer functions $f_{ij}^{(1)}(t)$ are²⁰

$$\begin{aligned}
 f_{11}^{(1)}(t) &= A_{2s} \exp\left(-\frac{t}{T_{2s}}\right) + A_{2f} \exp\left(-\frac{t}{T_{2f}}\right), \\
 f_{13}^{(1)}(t) = f_{31}^{(1)}(t) &= \frac{\sqrt{6}}{5} \left(\exp\left(-\frac{t}{T_{2f}}\right) - \exp\left(-\frac{t}{T_{2s}}\right) \right) \\
 f_{33}^{(1)}(t) &= A_{2f} \exp\left(-\frac{t}{T_{2s}}\right) + A_{2s} \exp\left(-\frac{t}{T_{2f}}\right)
 \end{aligned} \tag{8}$$

where the slow and fast relaxation times are $T_{2s} = \frac{1}{(J_1+J_2)}$ and $T_{2f} = \frac{1}{(J_0+J_1)}$, respectively. The theoretical amplitudes for the slow and fast components correspond to $A_{2s} = 0.4$ and $A_{2f} = 0.6$, respectively.

Hence, both transversal and longitudinal evolution yield Rank 3 coherence, which can be transferred to T_{33} TQ coherence by applying RF pulses. However, each pathway has its own sensitivity to the motional environment. While J_1 and J_2 are similar and have their largest difference for correlation times close to the inverse of the Larmor frequency, J_0 is linear in τ_c and is therefore particularly sensitive to slow motion. Only T_{2f} depends on J_0 . Hence, the difference between the T_2 relaxation times, which determines the T_2 -TQ signal, is dominated by slow motion with $\omega_0\tau_c \gtrsim 1$. The T_1 relaxation times only depend on J_1 and J_2 , and therefore the T_1 -TQ signal is dominated by an intermediate motional regime with $\omega_0\tau_c \sim 1$. Furthermore, determination of T_1 relaxation times is more challenging, as the fast T_1 component contributes only 20% to the overall signal.

The nuclear quadrupole strength parameter ω_Q and the correlation time τ_c can be calculated using both the T_1 and T_2 relaxation times.^{18,20,47} Using the T_1 relaxation times, they are

$$\tau_c = \frac{1}{\omega_0} \sqrt{\frac{a_0 - 1}{4 - a_0}} \quad \text{and} \quad \omega_Q = \sqrt{\frac{5b_0}{6x\tau_c} (4x^2 + 5x + 1)} \tag{9}$$

where $x = (\omega_0\tau_c)^2$, $a_0 = \frac{J_1}{J_2} = \frac{T_{1s}}{T_{1f}}$ and $b_0 = T_{1f}^{-1} - T_{1s}^{-1} = 2(J_1 - J_2)$. Using the T_2 relaxation times, they are

$$\tau_c = \frac{1}{\omega_0} \sqrt{\frac{1}{8} \left(5a_1 - 9 + \sqrt{25a_1^2 - 58a_1 + 49} \right)} \quad \text{and} \quad \omega_Q = \sqrt{\frac{5b_1(4x+1)}{4x\tau_c}} \tag{10}$$

where $a_1 = \frac{T_{2s}}{T_{2f}} = \frac{J_0+J_1}{J_1+J_2}$ and $b_1 = T_{2f}^{-1} - T_{2s}^{-1} = J_0 - J_2$.

B_0 inhomogeneities can influence relaxation by shifting the Larmor frequency locally. The effect of B_0 inhomogeneities on the transfer functions $f_{ij}^{(q)}$ can be described by^{40,48}

$$f_{ij,B0}^{(q)}(t) = f_{ij}^{(q)}(t) \int_{-\infty}^{\infty} p(\omega_{\text{shift}}) \exp(-iq\omega_{\text{shift}}t) d\omega_{\text{shift}} = f_{ij}^{(q)}(t) \exp(-qR_{B0}t), \tag{11}$$

where $p(\omega_{\text{shift}})$ is the distribution of ω_{shift} values and q is the coherence order. B_0 inhomogeneities usually follow a Lorentz distribution.^{40,49} The integral is the Fourier transform (FT) of $p(\omega_{\text{shift}})$ and the FT of a Lorentz distribution leads to an exponential free induction decay (FID). Therefore, the overall effect of B_0 inhomogeneity can be described as an additional coherence order dependent contribution to the relaxation rates R_i :

$$R_{i,B0} = R_i + qR_{B0}. \tag{12}$$

Here T_2 relaxation ($q = 1$) becomes T_2^* relaxation, while B_0 inhomogeneity does not affect T_1 relaxation ($q = 0$).

3 | METHODS

3.1 | IRTQTPPI pulse sequence and optimized phase cycles

The IRTQTPPI is a three-pulse sequence as shown in Figure 1. The 180° inversion pulse flips the equilibrium magnetization to the state described by $-T_{10}$, which evolves to the T_{30} state in the subsequent evolution period τ_{evo} . The second RF pulse with flip angle 90° transforms the T_{30} state to the TQ coherences T_{33} . Immediately afterwards, the third RF pulse, also with flip angle of 90° , transforms the T_{33} coherence into T_{31} coherence. This state evolves later to the MR detectable T_{11} coherence during the acquisition window. The phases of the standard sequence PC0 are $\phi_1 = 0$ for the first RF pulse, $\phi_1 = 90^\circ + 45^\circ n$ with $n = 1, \dots, 8$ and $\phi_3 = \phi_{\text{RX}} = 0$ for the last RF pulse and the receiver, respectively. In every phase step the evolution time τ_{evo} between the first and second RF pulses is incremented.

Imperfect RF pulses may lead to the creation of unwanted MR signal contributions (for example, DQ signal).³ For improved quantification of T_1 relaxation times and T_1 -TQ signal, three different phase cycles were evaluated for optimum reduction of unwanted signal contributions.

Phase cycle PC1 counteracts an imperfect inversion pulse by altering the phase of the inversion pulse by 180° . The T_{10} tensor remains unaffected, while accidentally created T_{11} coherences accumulate a 180° phase difference and thus are cancelled.

Phase cycle PC2 alters the phase of the second pulse by $\pm 135^\circ$, which results in a cancelling of signal components with even coherence order differences $\Delta m = m - m' = 2n$ (n being an integer, here $n = 1$), such as the transition $\hat{T}_{30} \rightarrow \hat{T}_{3\pm 2}$ or $\hat{T}_{1\pm 1} \rightarrow \hat{T}_{1\mp 1}$. Here, the $\pm 135^\circ$ phase shifts add $\pm 2 \times 135^\circ n = \pm 270^\circ n$ phase adding up to in total $(540^\circ n) \bmod 360^\circ = 180^\circ$ phase difference. Since transitions with odd coherence order difference $\Delta m = m - m'$ accumulate a phase difference of $\Delta m 270^\circ$, signal is lost due to inefficient interference. In comparison to PC0 and PC1, the signal to noise ratio (SNR) is reduced by a factor of $1/\sqrt{2}$. Additionally, this method leads to a 90° phase shift between the SQ and TQ peaks, which may impact fit accuracy.

Phase cycle PC3 is a combination of PC1 and PC2. The phase of the first pulse is altered by 180° . Additionally, PC3 alters the phase of the second pulse by $\pm 135^\circ$. This cycle therefore counteracts imperfections of both the 180° inversion pulse and the 90° pulses. However, this combination doubles the scan time compared with PC1 and PC2.

3.2 | Signal output and nonlinear fit

Similarly to the TQTPPI sequence, the signal of the IRTQTPPI sequence consists of a stack of spectra of the FT transforms of every first dimension FID along the acquisition time axis. The second dimension yields another FID, which is a function of the evolution time and corresponding phase step increment. Thus, the final signal contains both the SQ and TQ signal at distinct frequencies. The FID signal in the second dimension can be described by

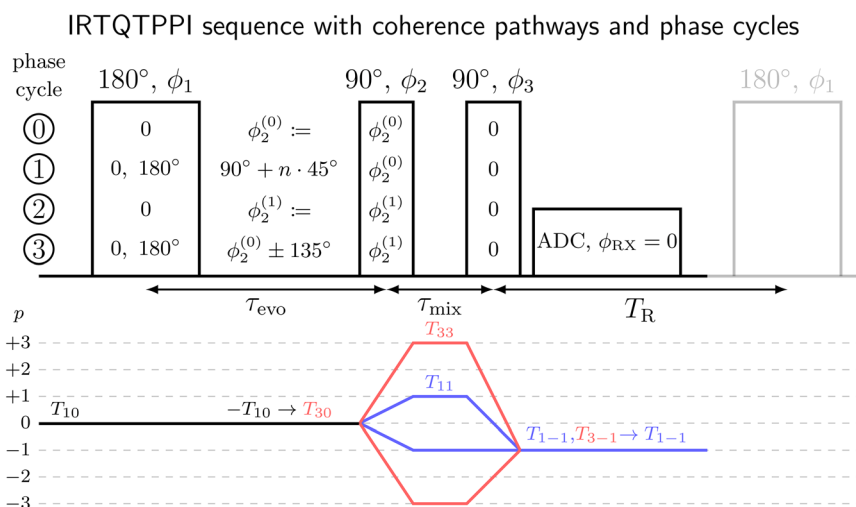


FIGURE 1 The IRTQTPPI pulse sequence and corresponding coherence pathways. The first 180° RF pulse inverts the longitudinal magnetization, which relaxes to T_{30} during the evolution period. The subsequent 90° RF pulse creates $T_{1\pm 1}$ SQ and $T_{3\pm 3}$ TQ coherences. The second 90° RF pulse transfers these states of magnetization to T_{1-1} and T_{3-1} , respectively. The following evolution converts T_{3-1} coherence to detectable T_{1-1} coherence, the evolution time τ_{evo} and the RF phases are simultaneously incremented. The initial evolution time increment $\Delta\tau_{\text{evo}}$ was non-equidistant with $8\Delta\tau_{\text{evo}}$ at a later time point to shorten acquisition time (Figure 2).

$$Y_1(t) = \sin(\omega t + \alpha_1) \left(1 - 2A_{1SQ} \left(A_{1s} e^{-\frac{t}{T_{1s}}} - A_{2f} e^{-\frac{t}{T_{1f}}} \right) \right) + A_{1TQ} \sin(3\omega t + \alpha_2) \left(e^{-\frac{t}{T_{1f}}} - e^{-\frac{t}{T_{1s}}} \right) + DC, \quad (13)$$

where $Y_1(t)$ is the IRTQTPPI FID amplitude. A_{1s} , A_{1f} and A_{1TQ} are the amplitudes of the slow and fast SQ signals as well as the TQ signal, respectively. $\omega = \frac{2\pi \Delta\phi}{360^\circ \Delta\tau_{evo}}$ is the frequency of the SQ signal determined by the phase cycle step. The values of α_1 and α_2 represent the phases of the SQ and TQ signals, respectively. The output FID in the second dimension was nonlinearly fitted by signal Equation 13. The total amplitude A_{1SQ} was used as a scaling factor accounting for imperfect inversion of magnetization. The amplitudes A_{1s} and A_{1f} of the slow and fast components were set to their theoretical values of 0.8 and 0.2, respectively.²⁰ Multiple studies^{22,50} have shown that the SQ amplitudes were close to their theoretical values for T_2 relaxation in agar samples and in vivo. Hence, it is reasonable to assume the same for T_1 relaxation. Moreover, fixed values were necessary to stabilize the fit results since the fast component contributes only 20% to the signal. We nevertheless evaluated the fit stability with bound and unbound amplitudes A_{1f} and A_{1s} .

A further improvement of fit accuracy and a reduction in measurement time were achieved in the IRTQTPPI sequence when two different evolution time increments were used. For small evolution times up to 65 ms, data was sampled more densely using a step of $\Delta\tau_{evo}$. For longer evolution times, data was sampled with a time step of $8\Delta\tau_{evo}$. <FIG 2>Figure 2 shows an exemplary FID in the second dimension with two evolution times. The FID in the second, evolution time, dimension is from now on referred to as FID.

3.3 | Experimental

Measurements were performed at a 9.4 T preclinical MRI scanner (BioSpec 94/20, Bruker, Ettlingen, Germany) and a 21.1 T preclinical MRI scanner at the National High Magnetic Field Laboratory (NHML, Tallahassee, FL, USA).⁵¹ At the 9.4 T scanner, we used a linear polarized $^1\text{H}/^{23}\text{Na}$ Bruker volume coil. Inner diameter and length were 72 and 100 mm for the ^{23}Na channel, respectively. At the 21.1 T, we used a custom-built $^1\text{H}/^{23}\text{Na}$ birdcage volume coil.⁵²

The samples contained [0, 2, 4, 6] % w/w agarose and 154 mM NaCl. Chemicals were purchased from Carl Roth (Karlsruhe, Germany). The samples were made by dissolving agarose in saline solution and heating the solution to 90 °C under stirring. After air bubbles left the heated solution, the solution was poured into 20 mL syringes. Syringes avoid a direct air contact, and this improved the B_0 shim. The resulting sample had 10 mL of solution, the sample diameter was 20 mm, and the height of the solution in the syringe was 35 mm.

The parameters of the IRTQTPPI sequence were $T_R = 400$ ms at 9.4 T ($T_R = 1$ s at 21.1 T), four averages at 9.4 T (one average at 21.1 T), $\Delta\tau_{evo} = 100$ μs and number of phase cycles with step of $\Delta\tau_{evo}$, $N_{PC} = 40$. The number of steps with $8\Delta\tau_{evo}$ was 300. To optimize the number of coarsely sampled data points, we varied the number of steps in the range of 0 to 320.

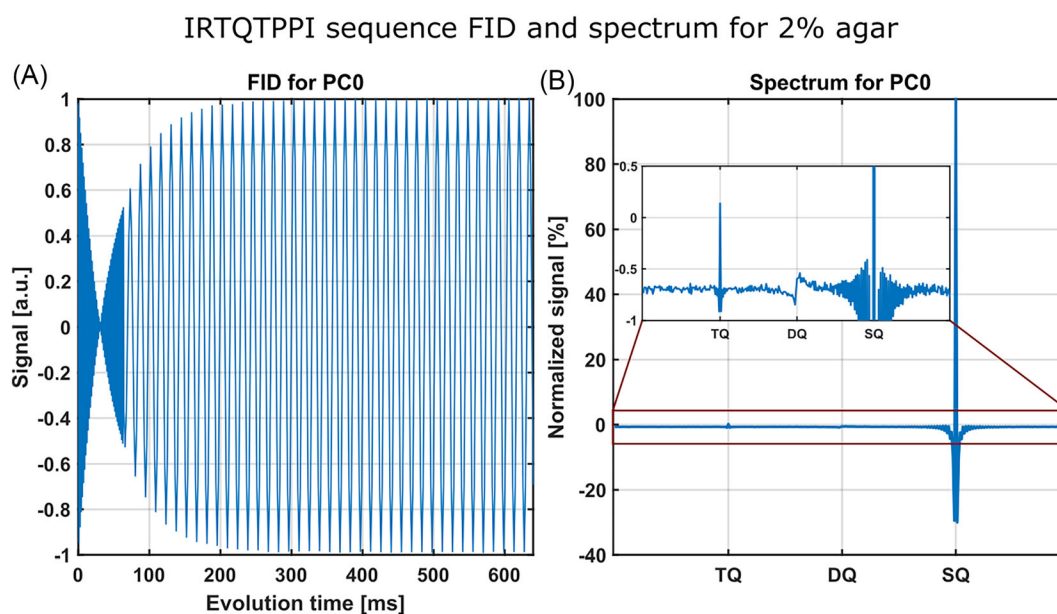


FIGURE 2 Sodium FID and spectrum of the 2% agar sample for phase cycle PC0 without DQ suppression at 9.4 T. A, The FID was sampled with two evolution time increments, $\Delta\tau_{evo}$ and $8\Delta\tau_{evo}$. B, The spectrum shows a TQ peak, which proved that T_1 relaxation was bi-exponential. A DQ peak could potentially affect the reliability of the fitting and hence DQ suppression methods were necessary.

The SNR of the TQ peak was determined by dividing the TQ peak height by the noise level. The noise level was determined by the standard deviation of the part of the spectrum that did not contain any signals.

We performed two stability tests of the IRTQTPPI method by determining the T_1 relaxation times and the T_1 -TQ signal. For the first stability test, we compared the fit results of all phase cycles. For the second test, we compared the fit results for varying numbers of points for the large evolution time increment $8 \Delta\tau_{\text{evo}}$.

For the T_2 -TQTPPI measurements, we used the TQTPPI sequence with a 180° refocusing pulse to compensate for B_0 inhomogeneities.^{22,33} The FID was fitted using the signal equation

$$Y_2(t) = \sin(\omega t + \alpha_1) \left(A_{2s} e^{-\frac{t}{T_{2s}}} - A_{2f} e^{-\frac{t}{T_{2f}}} \right) + A_{2\text{TQ}} \sin(3\omega t + \alpha_2) \left(e^{-\frac{t}{T_{2f}}} - e^{-\frac{t}{T_{2s}}} \right) + \text{DC} \quad (14)$$

where T_{2s} and T_{2f} are the slow and fast relaxation times, respectively. A_{2s} and A_{2f} are the amplitudes of the slow and fast components, respectively. $A_{2\text{TQ}}$ is the amplitude of the TQ signal. Other definitions are analogous to the definitions for $Y_1(t)$. The T_2 -TQ/SQ ratio is defined as

$$\frac{\text{TQ}}{\text{SQ}} = \frac{A_{2\text{TQ}}}{A_{2s} + A_{2f}}. \quad (15)$$

The standard deviations of the parameters were given by the fit uncertainties. The sequence parameters were $T_R = 400$ ms at 9.4 T ($T_R = 1$ s at 21.1 T), two averages at 9.4 T (one average at 21.1 T), number of phase cycles N_{PC} in the range of 60 to 100 and $\Delta\tau_{\text{evo}} = 200$ μs .

The T_1 -TQ/SQ ratio was determined in the same way as the T_2 -TQ/SQ ratio as

$$\frac{\text{TQ}}{\text{SQ}} = \frac{A_{1\text{TQ}}}{A_{1s} + A_{1f}}. \quad (16)$$

The $1 - 2f_{11}^{(0)}(t)$ behavior of the fit function in comparison to the TQTPPI pulse sequence makes the definition of the TQ/SQ ratio more complicated.

Many studies have used a mono-exponential approximation for T_1 relaxation.⁵³⁻⁶⁰ Therefore, we also calculated a mono-exponential approximation T_{1m} of the T_1 relaxation times using⁴⁹

$$T_{1m} = \frac{1}{\frac{0.8}{T_{1s}} + \frac{0.2}{T_{1f}}}. \quad (17)$$

The sensitivity to the motional environment is characterized by the typical time scale of motional averaging, the correlation time τ_c and the quadrupole interaction strength ω_Q . To investigate the motional regimes for both sequences, τ_c and ω_Q were calculated using Equations 9 and 10 for all pairs of T_1 and T_2 relaxation times, respectively.

4 | RESULTS

Figure 2 and <FIG 3>Figure 3 show spectra of all phase cycles at 9.4 T for the 2% agar sample. While phase cycle PC0 showed a DQ peak, phase cycles PC1, PC2 and PC3 successfully suppressed it. PC2 and PC3 shifted the phase of the TQ peak relative to the SQ peak by 90° . This resulted in the TQ peak pointing in the opposite direction compared with the corresponding SQ peak.

4.1 | Stability of IRTQTPPI fit results

The stability of the IRTQTPPI fitting results was evaluated using three different methods. The fitting results are shown in <TAB 1>Table 1 and <TAB 2>Table 2. First, we compared the fitting results with bound and unbound amplitudes A_{1f} and A_{1s} . The fit results with unbound amplitudes yielded large uncertainties and unrealistic amplitudes that strongly deviated from the theoretical values of $A_{1f} = 0.2$ and $A_{1s} = 0.8$. For the 2% and 4% agar samples, the fast amplitude contributed more than 90% instead of 20% to the overall SQ signal. Therefore, we used only the fit using bound A_{1f} and A_{1s} values.

Second, we compared the fit results for the different phase cycles. <FIG 4>Figure 4 and Table 2 show that for all samples and phase cycles the fit results for the relaxation times were consistent with each other. T_{1m} and T_{1s} almost perfectly matched for the different phase cycles, with

IRTQTPPI sequence spectra of all phase cycles for 2% agar

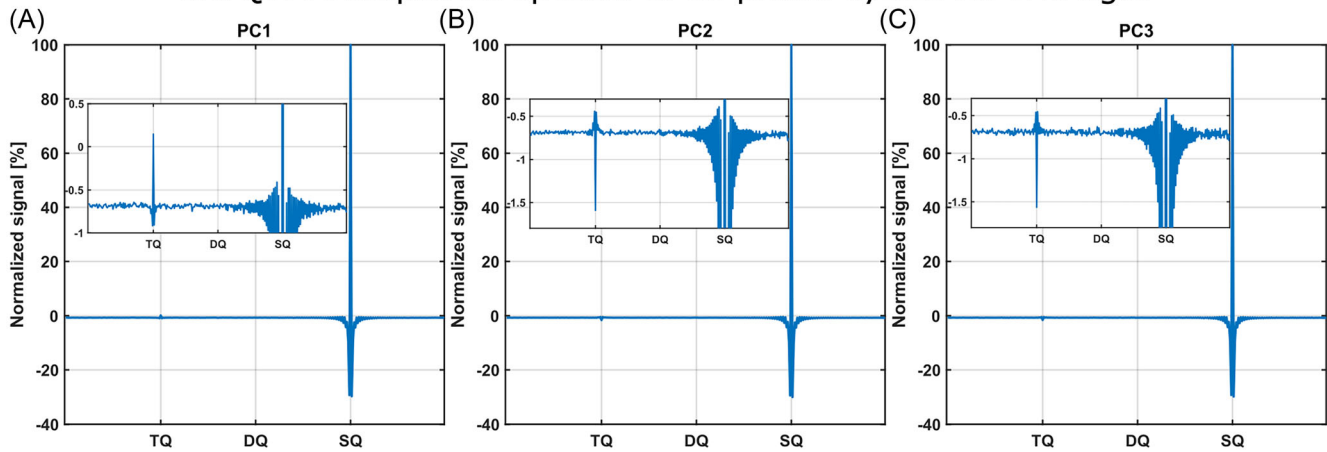


FIGURE 3 Comparison of all three DQ suppression methods, phase cycle PC1 (A), phase cycle PC2 (B) and phase cycle PC3 (C), for the 2% agar sample at 9.4 T. All three phase cycles effectively suppressed the DQ peak that was visible in the spectrum during phase cycle PC0, as shown in Figure 2. The TQ signal during PC2 and PC3 phase cycling accumulated an additional 90° phase shift relative to the SQ signal.

TABLE 1 Fit values for unbound SQ amplitudes A_{1s} and A_{1f} for phase cycle PC2 at 9.4 T. Both amplitudes strongly deviated from the theoretical values of $A_{1s} = 80\%$ and $A_{1f} = 20\%$ for the 2% and 4% agar samples. Furthermore, the T_{1s} relaxation time was close to the unrealistic upper bound of 100 ms and T_{1f} showed a large uncertainty.

Agar:	2%	4%	6%
T_{1s} [ms]	99.98 ± 0.40	99.99 ± 0.37	45.18 ± 1.57
T_{1f} [ms]	43.06 ± 12.28	41.27 ± 10.24	28.77 ± 3.51
T_{1m} [ms]	44.61 ± 12.45	43.04 ± 10.42	33.89 ± 6.92
A_{1s} [%]	5.45 ± 1.66	6.19 ± 1.50	38.64 ± 13.20
A_{1f} [%]	94.17 ± 1.69	93.33 ± 1.53	60.29 ± 13.24
TQ/SQ [%]	2.93 ± 0.42	3.42 ± 0.39	17.05 ± 3.62

deviations of less than 0.5 ms. The maximum deviation between the T_{1f} times of the different phase cycles was less than 1 ms. However, there was a substantial deviation of the T_1 -TQ/SQ ratios. Phase cycles PC0 and PC1 yielded approximately the same T_1 -TQ/SQ ratio, but this was substantially lower than the T_1 -TQ/SQ ratios of PC2 and PC3.

As the fit results for the relaxation times of all phase cycles were very similar, we chose phase cycle PC2 for all further measurements.

In the third stability test, we varied the number of data points with the larger evolution time increment of $8 \Delta\tau_{ev}$. <FIG 5>Figure 5 shows the relaxation times and the TQ signal in dependence on the number of points with large evolution time increment for the 2% agar sample. For all samples, both the T_1 -TQ/SQ ratio and the T_1 relaxation times showed a large variation for a low number of additional points. However, between 100 and 200 additional points, the fit converged to a stable set of parameters. For all further measurements, we set the number of additional points to 300.

4.2 | Comparison of T_1 and T_2 relaxation times and T_1 - and T_2 -TQ signals at 9.4 and 21.1 T

For all samples, both T_1 and s_2 relaxation were bi-exponential at 9.4 and 21.1 T, as shown in Figure 6. At 9.4 T, the separation in relaxation times was in the range of 15–18 ms for T_1 and 28–35 ms for T_2 . At 21.1 T it was in the range of 15–21 ms for T_1 and 37–40 ms for T_2 . In general, the uncertainties for the T_1 relaxation times were larger.

The T_1 -TQ/SQ ratio was smaller than the T_2 -TQ/SQ ratio. Both the T_1 - and T_2 -TQ/SQ ratio increased almost linearly with concentration with almost the same slope.

Increasing the magnetic field strength from 9.4 to 21.1 T led to increasing T_1 and T_2 relaxation times for all samples. Yet, both the T_1 -TQ and T_2 -TQ signals decreased despite larger T_1 and T_2 splitting.

TABLE 2 Comparison of the fit parameters using the IRTQTPPI sequence with the different phase cycles PC0, PC1, PC2 and PC3 at 9.4 T. The SQ amplitudes A_{1s} and A_{1f} were bound to their theoretical values of 0.8 and 0.2, respectively.

Agar:		2%	4%	6%
PC0	T_{1s} [ms]	49.44 ± 0.96	43.79 ± 1.18	37.50 ± 1.70
	T_{1f} [ms]	29.92 ± 0.31	25.67 ± 0.37	23.94 ± 0.50
	T_{1m} [ms]	43.78 ± 0.62	38.65 ± 0.75	34.00 ± 1.13
	TQ/SQ [%]	3.14 ± 0.53	5.77 ± 0.87	11.78 ± 2.37
PC1	T_{1s} [ms]	49.55 ± 0.90	43.62 ± 1.22	37.51 ± 1.66
	T_{1f} [ms]	30.19 ± 0.29	26.32 ± 0.38	23.75 ± 0.49
	T_{1m} [ms]	44.18 ± 0.59	38.92 ± 0.79	34.02 ± 1.10
	TQ/SQ [%]	3.09 ± 0.50	6.00 ± 0.93	11.47 ± 2.25
PC2	T_{1s} [ms]	49.22 ± 0.73	43.92 ± 0.98	37.92 ± 0.90
	T_{1f} [ms]	30.87 ± 0.23	25.65 ± 0.31	22.90 ± 0.27
	T_{1m} [ms]	44.10 ± 0.48	38.65 ± 0.75	33.91 ± 0.58
	TQ/SQ [%]	5.32 ± 0.48	8.67 ± 0.89	15.87 ± 1.50
PC3	T_{1s} [ms]	49.21 ± 0.81	43.78 ± 0.98	37.78 ± 0.86
	T_{1f} [ms]	30.87 ± 0.26	25.83 ± 0.31	23.09 ± 0.26
	T_{1m} [ms]	44.12 ± 0.53	38.76 ± 0.63	33.89 ± 0.56
	TQ/SQ [%]	5.34 ± 0.53	8.84 ± 0.91	15.86 ± 1.45

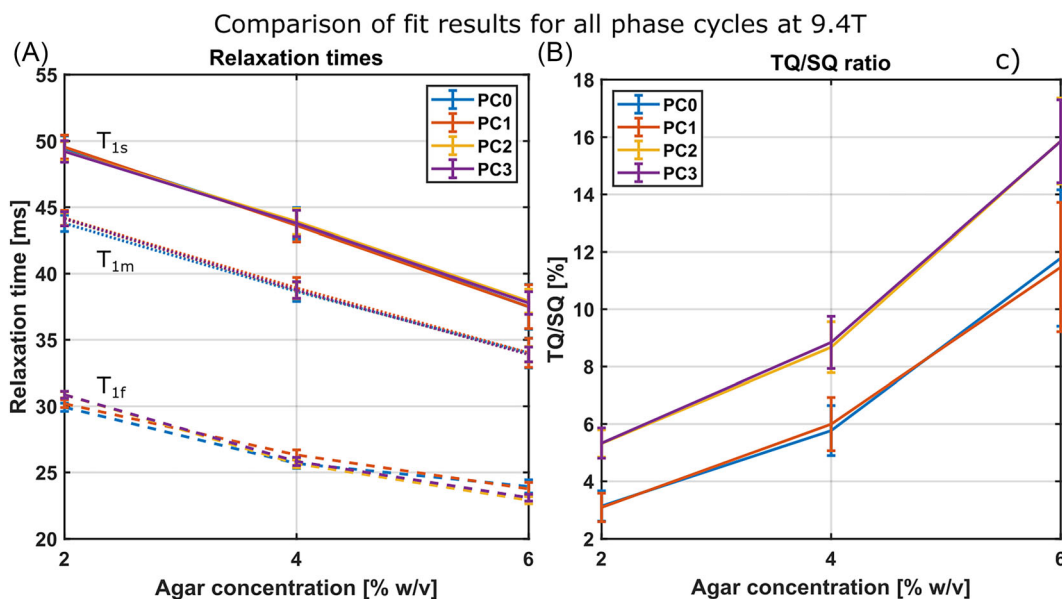


FIGURE 4 Comparison of fit parameters, T_1 relaxation times (A) and IR-TQ/SQ ratios (B), for all phase cycles using IRTQTPPI pulse sequence at 9.4 T. The relaxation times T_{1s} , T_{1f} and T_{1m} were in close agreement for all phase cycles. The T_1 -TQ/SQ ratios between PC0 and PC1 phase cycling were in close agreement as well as the ratios between PC2 and PC3. However, there was a substantial difference between these two pairs.

Figure 7 shows the correlation times τ_c and quadrupole strength parameters ω_Q calculated using the T_1 and T_2 relaxation times for 9.4 and 21.1 T. ω_Q is larger at 21.1 T and slightly increasing for increasing agar concentration. The slope was steeper for the quadrupole strength parameters calculated with the T_2 relaxation times. The correlation time was almost constant with increasing agar concentration for the T_1 parameters. In contrast, the correlation time was increasing with agar concentration for the T_2 parameters. τ_c was larger at 9.4 T than at 21.1 T, while ω_Q was larger at 21.1 T compared with 9.4 T.

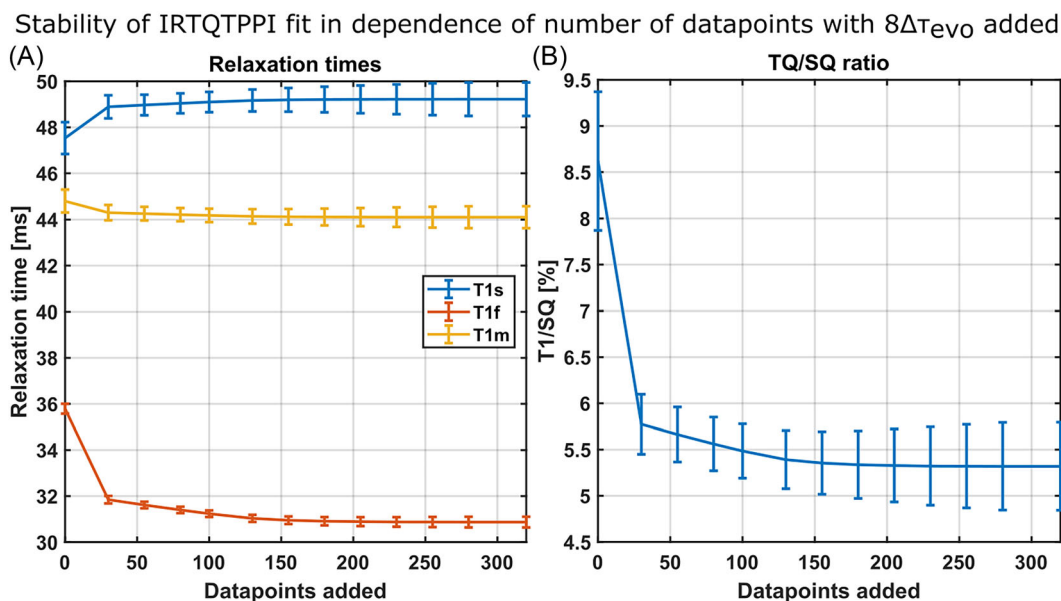


FIGURE 5 Dependence of the relaxation times (A) and the T_1 -TQ/SQ ratio (B) on the addition of the data points with an evolution time step of $8\Delta\tau_{\text{evo}}$ in the 2% agar sample using IRTQTPPI with phase cycle PC2 at 9.4 T. All fit parameters converged to stable values after addition of approximately 100–200 data points. Comparable results were observed for the other agarose samples.

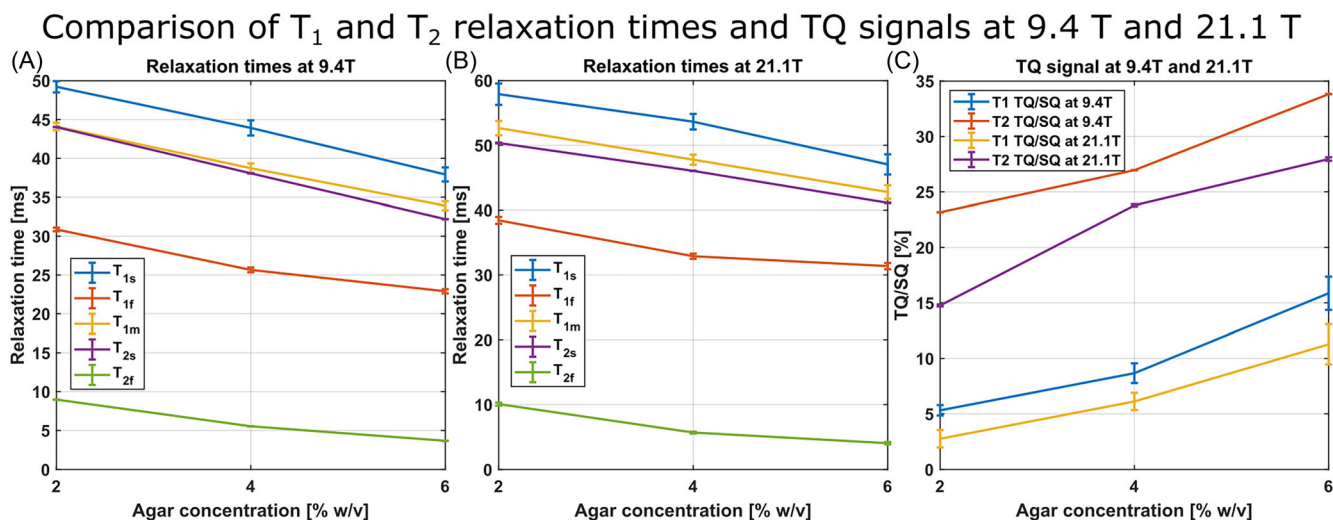


FIGURE 6 Comparison of sodium TQ/SQ and T_1 , T_2 relaxation times for the IRTQTPPI and TQTPPI pulse sequences at 9.4 and 21.1 T. At both magnetic field strengths, all agarose samples yielded a T_1 -TQ signal and bi-exponential T_1 relaxation times. As expected from theory, the T_2 pathway yielded a larger TQ signal and faster bi-exponential relaxation than T_1 pathway. The TQ signals of both pathways were smaller at the higher magnetic field strength.

5 | DISCUSSION

So far, the knowledge about bi-exponential ^{23}Na T_1 relaxation times of biological tissue is limited, as the fast component contributes only 20% to the total SQ signal and the difference in T_1 relaxation times can be rather small. Therefore, previous studies mainly approximated T_1 relaxation by a mono-exponential function.^{53–60} However, a reliable determination of both T_1 values is of importance for methods such as magnetic resonance fingerprinting.^{48,49,61} Furthermore, the unique sensitivity of the T_1 -TQ signal to the intermediate motional regime provides additional insights about the sodium molecular environment. In this study, we proposed a reliable method for the simultaneous quantification of the T_1 relaxation times and the T_1 -TQ signal.

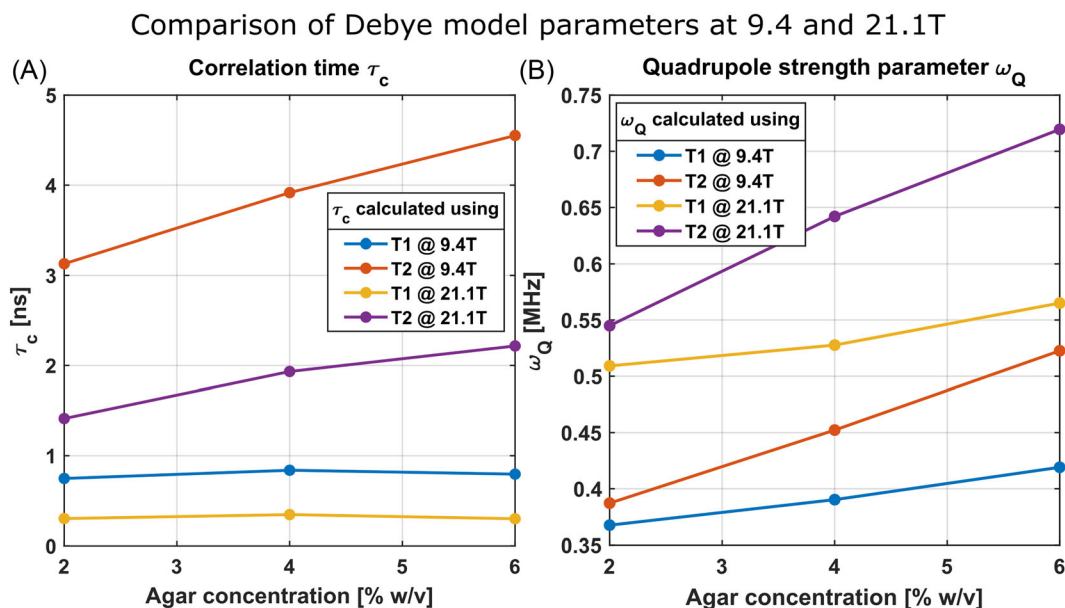


FIGURE 7 Comparison of the correlation times τ_c and the quadrupole interaction strengths ω_Q calculated from T_1 and the T_2 relaxation times measured at 9.4 and 21.1 T according to Equations 9 and 10.

For a reliable quantification of T_1 and T_1 -TQ values, we optimized the IRTQPPI sequence in three steps. (1) Fixation of the relative contribution of the fast and slow signal component. (2) Nonlinear sampling of the evolution time. (3) Suppression of unwanted signals.

The stability test showed that it was more crucial for the fit stability to sample the FID for sufficiently large τ_{evo} , to reduce the number of fit parameters and set the SQ amplitudes to their fixed theoretical values A_{1s} and A_{1f} . If the actual amplitudes deviated from the theoretical amplitudes, this could introduce errors in the determination of the relaxation times and other fit parameters. Several studies^{22,50} have demonstrated for T_2 relaxation that the theoretical amplitudes were close to their theoretical amplitudes in agar samples and even in vivo, suggesting that the fixed amplitude assumption may also be used in in vivo spectroscopy and imaging. Other studies have also stabilized the T_2 fit by using fixed amplitudes.^{48,62–64} The two T_1 relaxation times are close in value and much larger than the T_{2f} counterpart. Therefore, they are less affected by signal decay before the first echo/inversion. Hence, it is reasonable to assume that fixed T_1 amplitudes introduce less error than for T_2 .

Nonlinear sampling of the evolution time allowed us to avoid unreasonably long measurement times by using a second larger τ_{evo} increment. The number of data points with the increased τ_{evo} increment was varied to test the stability of the fit. For all samples and fit parameters, the fit stabilized and converged to a fixed set of parameters for a minimum of 100–200 additional data points.

For suppression of unwanted signals, we evaluated four different phase cycles for creation of the T_1 -TQ signal. In general, all phase cycles yielded similar T_1 relaxation times, and only the T_1 -TQ/SQ ratio was altered. A large unsuppressed DQ peak may affect fit accuracy. Only PC0 did not suppress the DQ peak; however, in these cases it did not influence the fit result substantially. The other phase cycles showed a similar effectiveness in suppression of the DQ signal. PC1 suppresses signal contributions from an imperfect 180° inversion RF pulse, while PC2 focusses on suppression of contributions with an even change in coherence order. PC3 combines the two phase cycles, doubling the scan time. The SQ signal of PC2 and PC3 did not perfectly constructively interfere, leading to a lower SQ signal and consequently a larger normalized TQ signal. The larger normalized TQ signal may make the extraction of small TQ signals easier. Transitions other than the desired T_1 pathway can create not only a DQ signal but also additional contributions to the SQ and TQ signals. For the SQ peak, these contributions should be much smaller than the signal from the $T_{10} \rightarrow T_{11}$ transition and therefore should not substantially influence the SQ peak. Alternative pathways that create a TQ peak, however, could in principle alter the TQ peak. As, for instance, Madelin et al.³ pointed out, the T_1 - and T_2 -TQ signals were not distinguishable in the case of imperfect flip angles. For our sequence, the only transitions that could create a TQ signal, that is, change in the coherence order by 3, were the $T_{30} \rightarrow T_{33}$ transition (T_1 -TQ signal) and the $T_{3\pm 1} \rightarrow T_{3\mp 2}$ transitions. In theory, both PC1 and PC3 corrected these contributions to the TQ signal by filtering out all contributions originating from T_{11} coherences created after an imperfect inversion pulse. In PC2, this pathway contributed to the signal. Nevertheless, the fit results almost perfectly matched between PC2 and PC3. Thus, the influence of this pathway should be negligible. Since PC2 and PC3 yielded a larger T_1 -TQ/SQ signal compared with PC1 and a shorter scan time compared with PC3, we used PC2 in all further measurements.

The T_1 pathway is sensitive to the difference in J_1 and J_2 and thus an intermediate motional regime. In the T_2 pathway, T_{2s} is sensitive to J_1 and J_2 , while the J_0 dependence of T_{2f} leads to a strong sensitivity to the slow-motion regime. Therefore, it is expected that the T_2 -TQ signal and the separation of the T_2 relaxation times is stronger than those for the T_1 pathway, which was confirmed by our measurements. Both

measurements enabled the characterization of the motional environment of the sodium nuclei by calculating the correlation times τ_c and quadrupole strength parameters ω_Q . In our measurements, both values did not match between the two pathways, which agrees with literature.^{3,18,19} Only in the case of a motional regime with a single τ_c and ω_Q do the τ_c and ω_Q values of the two pathways match independent of the calculation method and B_0 . In general, the motional regime is more accurately described by a distribution of correlation times and quadrupole strength parameters.^{18,19} Nevertheless, the simplified model still allows extraction of qualitative and effective information about the motional environment of the nuclei. The T_1 correlation time was almost constant with increasing agar concentration, in agreement with the sensitivity to interactions in the intermediate motional regime. On the other hand, the T_2 correlation time was increasing linearly with the agar concentration, as expected from theory. The $T_1 \omega_Q$ was increasing more slowly with agar concentration than the $T_2 \omega_Q$. This might indicate that with increasing agar concentration slow interactions become stronger and more frequent, while intermediate interactions are not affected as much. Moreover, all samples yielded a strong T_1 -TQ signal that increased with agar concentration with almost the same slope as the T_2 -TQ signal. The similar increase in T_1 - and T_2 -TQ signal combined with the dependence of the T_1 and T_2 correlation times indicated that the fractions of interactions in the intermediate and slow-motion regimes increased similarly.

In theory, the TQ/SQ ratio is expected to increase with B_0 since the intermediate ($\tau_c \omega_Q \sim 1$) and slow-motion ($\tau_c \omega_Q \gtrsim 1$) regimes are shifted toward smaller correlation times.²⁰ This agrees with the lower correlation time at 21.1 T. Nonetheless, in our measurements, the TQ/SQ ratios decreased at 21.1 T compared with 9.4 T. This suggested a strong influence of B_0 and B_1 inhomogeneities on the TQ signal.⁴⁰ In general, B_0 and B_1 inhomogeneities increase with field strength. Both T_1 -TQ and T_2 -TQ signals strongly depend on the flip angle accuracy and B_1 homogeneity. The T_2 -TQ signal has a flip angle dependence of $\sin^5(\theta)$.³⁸ Similarly, the T_1 -TQ flip angle dependence can be calculated using the Wigner matrix elements: the flip angle dependence is $\cos(\theta_1) \sin^5(\theta_2)$, where θ_1 is the flip angle of the inversion pulse and θ_2 is the flip angle of the second and third pulses. Since RF absorption increases with B_0 , B_1 inhomogeneity is expected to increase and therefore increasing field strength does not necessarily improve the TQ signal as theoretically expected. Moreover, the increased RF absorption increases specific absorption rate (SAR) and necessitates longer T_R , which increases scan time.

The IRTQTPPI sequence can also be used with an imaging sequence similar to the TQTPPI sequence⁶⁵⁻⁶⁷ and TQF sequences.^{26,36} These sequences use a fixed evolution time and a sampling of the T_2 -TQ signal at the maximum, which can also be done with the IRTQTPPI sequence. To extract the T_1 relaxation times, an evolution time increment must be used. Sparsity in the multidimensional data could be exploited in the way that Licht et al. proposed for their sequence⁶⁷ to optimize scan time. One drawback of T_1 -TQ was the smaller signal compared with T_2 -TQ, which is already only one-tenth of the SQ signal. The lower SNR might also affect the accuracy and robustness of the T_1 relaxation time quantification. Since the contribution of the T_{1f} signal is only 20%, an SNR higher than for T_2 quantification may be required. To achieve high SNR in reasonable scan time, sparsity could be exploited, similarly to the approach of Licht et al.⁶⁷ Furthermore, the 180° pulse doubles the SAR compared with the 90° pulse. Consequently, the T_2 -TQ measurement will be a better choice for clinical applications due to the higher SNR and lower SAR. Nevertheless, the IRTQTPPI sequence still improves the characterization of the motional environment and T_1 relaxation behavior of the sodium nuclei.

6 | CONCLUSION

In this study, a reliable method for simultaneous quantification of sodium T_1 -TQ signal, SQ signal and bi-exponential T_1 relaxation times was demonstrated. Combination of optimized fit parameters, nonuniform sampling of evolution time and suppression of unwanted signals resulted in reliable and stable IRTQTPPI measurements. At 9.4 and 21.1 T, all samples of the agar model system yielded a T_1 -TQ signal and bi-exponential sodium relaxation times. In contrast to theoretical expectations, the T_1 - and T_2 -TQ signals decreased with field strength, mostly due to B_0 and B_1 inhomogeneity. The T_2 -TQ signal and the T_1 -TQ signal represent different ranges of the sodium nucleus motion, as demonstrated for the agar tissue model system. The IRTQTPPI pulse sequence provides a less intensive TQ signal than TQTPPI. Altogether, the proposed IRTQTPPI sequence allows for an improved characterization of the sodium molecular environment.

ACKNOWLEDGEMENTS

A portion of this work was performed at the National High Magnetic Field Laboratory, which is supported by National Science Foundation Cooperative Agreement DMR-1644779 and the State of Florida. Part of this work was supported by the German Research Foundation (Grant 410981386). Open Access funding enabled and organized by Projekt DEAL.

CONFLICT OF INTEREST STATEMENT

The authors have no conflict of interest to declare.

ORCID

Simon Reichert  <https://orcid.org/0000-0002-6013-8242>

Dennis Kleimaier  <https://orcid.org/0000-0002-7885-7675>

REFERENCES

- Hu R, Kleimaier D, Malzacher M, Hoesl MAU, Paschke NK, Schad LR. X-nuclei imaging: current state, technical challenges, and future directions. *J Magn Reson Imaging*. 2020;51(2):355-376. doi:10.1002/jmri.26780
- Thulborn KR. Quantitative sodium MR imaging: a review of its evolving role in medicine. *Neuroimage*. 2018;168:250-268. doi:10.1016/j.neuroimage.2016.11.056
- Madelin G, Lee J-S, Regatte RR, Jerschow A. Sodium MRI: methods and applications. *Prog Nucl Magn Reson Spectrosc*. 2014;79:14-47. doi:10.1016/j.pnmrs.2014.02.001
- Alberts B, Johnson A, Lewis J, Raff M, Roberts K, Walter P. *Molecular Biology of the Cell*. 5th ed. Garland Science; 2008:1121-1128.
- Clausen MV, Hilbers F, Poulsen H. The structure and function of the Na,K-ATPase isoforms in health and disease. *Rev Front Physiol*. 2017;8:371. doi:10.3389/fphys.2017.00371
- Lachner S, Ruck L, Niesporek SC, et al. Comparison of optimized intensity correction methods for ²³Na MRI of the human brain using a 32-channel phased array coil at 7 Tesla. *Z Med Phys*. 2020;30(2):104-115. doi:10.1016/j.zemedi.2019.10.004
- Malzacher M, Chacon-Caldera J, Paschke N, Schad LR. Feasibility study of a double resonant (¹H/²³Na) abdominal RF setup at 3T. *Z Med Phys*. 2019;29(4):359-367. doi:10.1016/j.zemedi.2018.12.004
- Rooney WD, Li X, Sammi MK, Bourdette DN, Neuwelt EA, Springer CS Jr. Mapping human brain capillary water lifetime: high-resolution metabolic neuroimaging. *NMR Biomed*. 2015;28(6):607-623. doi:10.1002/nbm.3294
- Dizon JM, Tauskela JS, Wise D, Burkhoff D, Cannon PJ, Katz J. Evaluation of triple-quantum-filtered ²³Na NMR in monitoring of intracellular Na content in the perfused rat heart: comparison of intra- and extracellular transverse relaxation and spectral amplitudes. *Magn Reson Med*. 1996;35(3):336-345. doi:10.1002/mrm.1910350311
- Eykyn TR, Aksentijević D, Aughton KL, Southworth R, Fuller W, Shattock MJ. Multiple quantum filtered ²³Na NMR in the Langendorff perfused mouse heart: ratio of triple/double quantum filtered signals correlates with [Na]_i. *J Mol Cell Cardiol*. 2015;86:95-101. doi:10.1016/j.yjmcc.2015.07.009
- Jelicks LA, Gupta RK. On the extracellular contribution to multiple quantum filtered ²³Na NMR of perfused rat heart. *Magn Reson Med*. 1993;29(1):130-133. doi:10.1002/mrm.1910290124
- Knubovets T, Shinar H, Navon G. Quantification of the contribution of extracellular sodium to ²³Na multiple-quantum-filtered NMR spectra of suspensions of human red blood cells. *J Magn Reson*. 1998;131(1):92-96. doi:10.1006/jmre.1997.1337
- Schepkin VD, Choy IO, Budinger TF. Sodium alterations in isolated rat heart during cardioplegic arrest. *J Appl Physiol*. 1996;81(6):2696-2702. doi:10.1152/jappl.1996.81.6.2696
- Schepkin VD, Choy IO, Budinger TF, et al. Sodium TQF NMR and intracellular sodium in isolated crystalloid perfused rat heart. *Magn Reson Med*. 1998;39(4):557-563. doi:10.1002/mrm.1910390408
- Seshan V, Sherry AD, Bansal N. Evaluation of triple quantum-filtered ²³Na NMR spectroscopy in the in situ rat liver. *Magn Reson Med*. 1997;38(5):821-827. doi:10.1002/mrm.1910380519
- Winter PM, Bansal N. Triple-quantum-filtered ²³Na NMR spectroscopy of subcutaneously implanted 9L gliosarcoma in the rat in the presence of TmDOTP⁵⁻. *J Magn Reson*. 2001;152(1):70-78. doi:10.1006/jmre.2001.2390
- Schepkin VD. Statistical tensor analysis of the MQ MR signals generated by weak quadrupole interactions. *Z Med Phys*. 2019;29(4):326-336. doi:10.1016/j.zemedi.2019.03.002
- Rooney WD, Springer CS. A comprehensive approach to the analysis and interpretation of the resonances of spins 3/2 from living systems. *NMR Biomed*. 1991;4(5):209-226. doi:10.1002/nbm.1940040502
- Rooney WD, Springer CS Jr. The molecular environment of intracellular sodium: ²³Na NMR relaxation. *NMR Biomed*. 1991;4(5):227-245. doi:10.1002/nbm.1940040503
- van der Maarel JRC. Thermal relaxation and coherence dynamics of spin 3/2. I. Static and fluctuating quadrupolar interactions in the multipole basis. *Concepts Magn Reson*. 2003;19A(2):97-116. doi:10.1002/cmr.a.10087
- van der Maarel JRC. Thermal relaxation and coherence dynamics of spin 3/2. II. Strong radio-frequency field. *Concepts Magn Reson A*. 2003;19A(2):117-133. doi:10.1002/cmr.a.10088
- Schepkin VD, Neubauer A, Nagel AM, Budinger TF. Comparison of potassium and sodium binding in vivo and in agarose samples using TQTPPI pulse sequence. *J Magn Reson*. 2017;277:162-168. doi:10.1016/j.jmr.2017.03.003
- Choy IO, Schepkin VD, Budinger TF, Obayashi DY, Young JN, DeCampli WM. Effects of specific sodium/hydrogen exchange inhibitor during cardioplegic arrest. *Ann Thorac Surg*. 1997;64(1):94-99. doi:10.1016/S0003-4975(97)00245-2
- Schepkin VD, Choy IO, Budinger TF, Young JN, DeCampli WM. Multi-dose crystalloid cardioplegia preserves intracellular sodium homeostasis in myocardium. *J Mol Cell Cardiol*. 1999;31(9):1643-1651. doi:10.1006/jmcc.1999.1002
- Tauskela JS, Dizon JM, Whang J, Katz J. Evaluation of multiple-quantum-filtered ²³Na NMR in monitoring intracellular Na content in the isolated perfused rat heart in the absence of a chemical-shift reagent. *J Magn Reson*. 1997;127(1):115-127. doi:10.1006/jmre.1997.1181
- LaVerde G, Nemoto E, Jungreis CA, Tanase C, Boada FE. Serial triple quantum sodium MRI during non-human primate focal brain ischemia. *Magn Reson Med*. 2007;57(1):201-205. doi:10.1002/mrm.21087
- Babsky AM, Zhang H, Hekmatyar SK, Hutchins GD, Bansal N. Monitoring chemotherapeutic response in RIF-1 tumors by single-quantum and triple-quantum-filtered ²³Na MRI, ¹H diffusion-weighted MRI and PET imaging. *Magn Reson Imaging*. 2007;25(7):1015-1023. doi:10.1016/j.mri.2006.11.004
- Winter PM, Poptani H, Bansal N. Effects of chemotherapy by 1,3-bis(2-chloroethyl)-1-nitrosourea on single-quantum- and triple-quantum-filtered ²³Na and ³¹P nuclear magnetic resonance of the subcutaneously implanted 9L glioma. *Cancer Res*. 2001;61(5):2002-2007.
- Gottwald E, Kleintschek T, Giselbrecht S, et al. Characterization of a chip-based bioreactor for three-dimensional cell cultivation via magnetic resonance imaging. *Z Med Phys*. 2013;23(2):102-110. doi:10.1016/j.zemedi.2013.01.003
- Hoesl MAU, Kleimaier D, Hu R, et al. ²³Na triple-quantum signal of in vitro human liver cells, liposomes, and nanoparticles: cell viability assessment vs. separation of intra- and extracellular signal. *J Magn Reson Imaging*. 2019;50(2):435-444. doi:10.1002/jmri.26666
- Kleimaier D, Schepkin V, Nies C, Gottwald E, Schad LR. Intracellular sodium changes in cancer cells using a microcavity array-based bioreactor system and sodium triple-quantum MR signal. *Processes*. 2020;8(10):1267. doi:10.3390/pr8101267s

32. Neubauer A, Nies C, Schepkin VD, et al. Tracking protein function with sodium multi quantum spectroscopy in a 3D-tissue culture based on microcavity arrays. *Sci Rep*. 2017;7(1):3943. doi:10.1038/s41598-017-04226-2
33. Kleimaier D, Schepkin V, Hu R, Schad LR. Protein conformational changes affect the sodium triple-quantum MR signal. *NMR Biomed*. 2020;33(10):e4367. doi:10.1002/nbm.4367
34. Bodenhausen G. Multiple-quantum NMR. *Prog Nucl Magn Reson Spectrosc*. 1980;14(3):137-173. doi:10.1016/0079-6565(80)80007-0
35. Chung C-W, Wimperis S. Optimum detection of spin-3/2 biexponential relaxation using multiple-quantum filtration techniques. *J Magn Reson*. 1990;88(2):440-447. doi:10.1016/0022-2364(90)90204-M
36. Fiege DP, Romanzetti S, Mirkes CC, Brenner D, Shah NJ. Simultaneous single-quantum and triple-quantum-filtered MRI of ^{23}Na (SISTINA). *Magn Reson Med*. 2013;69(6):1691-1696. doi:10.1002/mrm.24417
37. Fleysher L, Oesingmann N, Inglese M. B0 inhomogeneity-insensitive triple-quantum-filtered sodium imaging using a 12-step phase-cycling scheme. *NMR Biomed*. 2010;23(10):1191-1198. doi:10.1002/nbm.1548
38. Hancu I, Boada FE, Shen GX. Three-dimensional triple-quantum-filtered ^{23}Na imaging of in vivo human brain. *Magn Reson Med*. 1999;42(6):1146-1154. doi:10.1002/(SICI)1522-2594(199912)42:6<3.0.CO;2-Ss
39. Navon G, Shinar H, Eliav U, Seo Y. Multiquantum filters and order in tissues. *NMR Biomed*. 2001;14(2):112-132. doi:10.1002/nbm.687
40. Tanase C, Boada FE. Triple-quantum-filtered imaging of sodium in presence of B0 inhomogeneities. *J Magn Reson*. 2005;174(2):270-278. doi:10.1016/j.jmr.2005.02.012
41. Jaccard G, Wimperis S, Bodenhausen G. Multiple-quantum NMR spectroscopy of $S=3/2$ spins in isotropic phase: a new probe for multiexponential relaxation. *J Chem Phys*. 1986;85(11):6282-6293. doi:10.1063/1.451458
42. Andrasko J. Nonexponential relaxation of $^{23}\text{Na}^+$ in agarose gels. *J Magn Reson*. 1974;16(3):502-504. doi:10.1016/0022-2364(74)90233-9
43. Boicelli CA, Giuliani AM. Sodium ion distribution in the vitreous body. *Magn Reson Mater Phys Biol Med*. 1996;4(3):241-245. doi:10.1007/BF01772012
44. Monoi H. Nuclear magnetic resonance of ^{23}Na ions interacting with the gramicidin channel. *Biophys J*. 1985;48(4):643-662. doi:10.1016/s0006-3495(85)83820-0
45. Hancu I, van der Maarel JRC, Boada FE. A model for the dynamics of spins 3/2 in biological media: signal loss during radiofrequency excitation in triple-quantum-filtered sodium MRI. *J Magn Reson*. 2000;147(2):179-191. doi:10.1006/jmre.2000.2177
46. Wu C, Blunck Y, Johnston LA. The "spin-3/2 Bloch equation": system matrix formalism of excitation, relaxation, and off-resonance effects in biological tissue. *Magn Reson Med*. 2022;88(3):1370-1379. doi:10.1002/mrm.29276
47. Matthias C. *Über den Einfluß von Inhomogenitäten im Grundmagnetfeld auf die Tripelquantengefilterte Natrium-MR-Spektroskopie und -Bildgebung*. Dissertation. Heidelberg University; 2010.
48. Kratzer FJ, Flassbeck S, Nagel AM, et al. Sodium relaxometry using ^{23}Na MR fingerprinting: a proof of concept. *Magn Reson Med*. 2020;84(5):2577-2591. doi:10.1002/mrm.28316
49. Kratzer FJ, Flassbeck S, Schmitter S, et al. 3D sodium (^{23}Na) magnetic resonance fingerprinting for time-efficient relaxometric mapping. *Magn Reson Med*. 2021;86(5):2412-2425. doi:10.1002/mrm.28873
50. Alhulail AA, Xia P, Shen X, et al. Fast in vivo ^{23}Na imaging and T_2^* mapping using accelerated 2D-FID UTE magnetic resonance spectroscopic imaging at 3 T: proof of concept and reliability study. *Magn Reson Med*. 2021;85(4):1783-1794. doi:10.1002/mrm.28576
51. Fu R, Brey WW, Shetty K, et al. Ultra-wide bore 900MHz high-resolution NMR at the National High Magnetic Field Laboratory. *J Magn Reson*. 2005;177(1):1-8. doi:10.1016/j.jmr.2005.07.013
52. Qian C, Masad IS, Rosenberg JT, et al. A volume birdcage coil with an adjustable sliding tuner ring for neuroimaging in high field vertical magnets: ex and in vivo applications at 21.1T. *J Magn Reson*. 2012;221:110-116. doi:10.1016/j.jmr.2012.05.016
53. Chang G, Madelin G, Sherman OH, et al. Improved assessment of cartilage repair tissue using fluid-suppressed ^{23}Na inversion recovery MRI at 7 Tesla: preliminary results. *Eur Radiol*. 2012;22(6):1341-1349. doi:10.1007/s00330-012-2383-8
54. Kline RP, Wu EX, Petrylak DP, et al. Rapid in vivo monitoring of chemotherapeutic response using weighted sodium magnetic resonance imaging. *Clin Cancer Res*. 2000;6(6):2146-2156.
55. Madelin G, Babb J, Xia D, et al. Articular cartilage: evaluation with fluid-suppressed 7.0-T sodium MR imaging in subjects with and subjects without osteoarthritis. *Radiology*. 2013;268(2):481-491. doi:10.1148/radiol.13121511
56. Madelin G, Babb JS, Xia D, Chang G, Jerschow A, Regatte RR. Reproducibility and repeatability of quantitative sodium magnetic resonance imaging in vivo in articular cartilage at 3 T and 7 T. *Magn Reson Med*. 2012;68(3):841-849. doi:10.1002/mrm.23307
57. Madelin G, Jerschow A, Regatte RR. Sodium MRI with fluid suppression: will it improve early detection of osteoarthritis? *Imaging Med*. 2011;3(1):1-4. doi:10.2217/iim.10.70
58. Madelin G, Lee J-S, Inati S, Jerschow A, Regatte RR. Sodium inversion recovery MRI of the knee joint in vivo at 7T. *J Magn Reson*. 2010;207(1):42-52. doi:10.1016/j.jmr.2010.08.003
59. Rong P, Regatte RR, Jerschow A. Clean demarcation of cartilage tissue ^{23}Na by inversion recovery. *J Magn Reson*. 2008;193(2):207-209. doi:10.1016/j.jmr.2008.04.036
60. Stobbe R, Beaulieu C. In vivo sodium magnetic resonance imaging of the human brain using soft inversion recovery fluid attenuation. *Magn Reson Med*. 2005;54(5):1305-1310. doi:10.1002/mrm.20696
61. Rodriguez GG, Yu Z, O'Donnell LF, Calderon L, Cloos MA, Madelin G. Repeatability of simultaneous 3D 1H MRF/ ^{23}Na MRI in brain at 7 T. *Sci Rep*. 2022;12(1):14156. doi:10.1038/s41598-022-18388-1
62. Blunck Y, Josan S, Taqdees SW, et al. 3D-multi-echo radial imaging of ^{23}Na (3D-MERINA) for time-efficient multi-parameter tissue compartment mapping. *Magn Reson Med*. 2018;79(4):1950-1961. doi:10.1002/mrm.26848
63. Paschke NK, Neumann W, Uhrig T, et al. Influence of gadolinium-based contrast agents on tissue sodium quantification in sodium magnetic resonance imaging. *Invest Radiol*. 2018;53(9):555-562. doi:10.1097/RLI.0000000000000487
64. Ridley B, Nagel AM, Bydder M, et al. Distribution of brain sodium long and short relaxation times and concentrations: a multi-echo ultra-high field ^{23}Na MRI study. *Sci Rep*. 2018;8(1):4357. doi:10.1038/s41598-018-22711-0
65. Hoesl MAU, Schad LR, Rapacchi S. Efficient ^{23}Na triple-quantum signal imaging on clinical scanners: Cartesian imaging of single and triple-quantum ^{23}Na (CRISTINA). *Magn Reson Med*. 2020;84(5):2412-2428. doi:10.1002/mrm.28284

66. Hoesl MAU, Schad LR, Rapacchi S. Volumetric ^{23}Na single and triple-quantum imaging at 7T: 3D-CRISTINA. *Z Med Phys.* 2022;32(2):199-208. doi:[10.1016/j.zemedi.2021.09.001](https://doi.org/10.1016/j.zemedi.2021.09.001)
67. Licht C, Reichert S, Guye M, Schad LR, Rapacchi S. Multidimensional compressed sensing to advance ^{23}Na multi-quantum coherences MRI. *Magn Reson Med.* 2023;91(3):926-941. doi:[10.1002/mrm.29902](https://doi.org/10.1002/mrm.29902)

How to cite this article: Reichert S, Schepkin V, Kleimaier D, Zöllner FG, Schad LR. Comparison of triple quantum (TQ) TPPI and inversion recovery TQ TPPI pulse sequences at 9.4 and 21.1 T. *NMR in Biomedicine.* 2024;37(5):e5106. doi:[10.1002/nbm.5106](https://doi.org/10.1002/nbm.5106).